



Original Article

# ALENDRONATE NANOPARTICLES PROMOTE FRACTURE HEALING BY INHIBITING LRP4 TO ACTIVATE THE WNT/ $\beta$ -CATENIN PATHWAY

Z.W. Sun<sup>1,§</sup>, Q.L. Zhu<sup>2,§</sup>, J.P. Gong<sup>1</sup>, Y.H. Sui<sup>2,\*</sup> and X.Y. Liu<sup>2,\*</sup>

 $^1$ Trauma Department 1, Yantaishan Hospital, 264000 Yantai, Shandong, China  $^2$ Pharmaceutical Department, Yantai Yuhuangding Hospital, 264000 Yantai, Shandong, China  $^\S$ These authors contributed equally.

#### Abstract

Background: Fracture is a common skeletal disorder, and fracture healing is a complex biological process. The Wingless-Int-Integrated/beta-catenin (Wnt/ $\beta$ -catenin) signaling pathway plays an important role in bone formation and fracture healing. Low-density lipoprotein receptor-related protein 4 (LRP4) has been reported to negatively regulate the Wnt/ $\beta$ -catenin pathway. This study investigated whether alendronate nanoparticles (alendronate-NPs) can activate the Wnt/\(\beta\)-catenin pathway by inhibiting LRP4, thereby promoting fracture healing. Methods: We initially synthesized alendronate-NPs. Then, the impact of alendronate, alendronate-NPs, and LRP4 on the osteogenic differentiation of rat osteoblasts was investigated. The proliferation capacity of osteoblasts was evaluated using cell-counting kit-8. The effects on the messenger ribonucleic acid (mRNA) and protein levels of proliferating cell nuclear antigen (PCNA), runt-related transcription factor 2 (Runx2), osteocalcin (OCN), osteopontin (OPN), LRP4, Wingless-type MMTV integration site family, member 4 (Wnt4), glycogen synthase kinase 3 beta (GSK-3 $\beta$ ), p-GSK-3 $\beta$ , and  $\beta$ -catenin were analyzed by quantitative reverse-transcription polymerase chain reaction and Western blot. The impact on osteoblast apoptosis and calcium deposition was assessed using terminal deoxynucleotidyl transferase-mediated dUTP nick end labeling (TUNEL) and alizarin red staining assays. A rat fracture model was then established, followed by treatments with either alendronate or alendronate-NPs. Bone formation during fracture healing was evaluated using alkaline phosphatase. The effects of alendronate and alendronate-NPs on fracture healing were assessed through hematoxylin-eosin (HE) staining and immunohistochemistry staining of collagen I. Results: Alendronate and alendronate-NPs significantly downregulated the expression of LRP4 during osteoblast differentiation and upregulated the expression of downstream targets of the Wnt/ $\beta$ -catenin pathway (p < 0.01). The co-treatment of osteoblasts with alendronate-NPs and LRP4 overexpression partially offset the bone-formation-promoting effects of alendronate-NPs. LRP4 overexpression reversed the proliferative and osteogenic effects of alendronate-NPs (p < 0.01). Compared with alendronate-NP treatment alone, the combined treatment of alendronate-NPs and LRP4 overexpression downregulated the expression of downstream targets of the Wnt/ $\beta$ -catenin pathway in osteoblasts (p < 0.01). Alendronate and alendronate-NPs significantly accelerated fracture healing in rats. They also promoted the proliferation and bone-formation capacity of osteoblasts, with alendronate-NPs showing a more pronounced therapeutic effect on fracture healing than alendronate. Conclusions: Alendronate-NPs may promote fracture healing by inhibiting LRP4 to activate the Wnt/ $\beta$ -catenin pathway. This study provides experimental evidence for a new mechanism of alendronate-NPs in promoting fracture healing.

**Keywords:** Alendronate nanoparticles, LRP4, Wnt/β-catenin pathway, bone-fracture healing.

\*Address for correspondence: Y.H. Sui, Pharmaceutical Department, Yantai Yuhuangding Hospital, 264000 Yantai, Shandong, China. E-mail: 13583544489@163.com; X.Y. Liu, Pharmaceutical Department, Yantai Yuhuangding Hospital, 264000 Yantai, Shandong, China. E-mail: 13553106682@163.com.

**Copyright policy**: © 2025 The Author(s). Published by Forum Multimedia Publishing, LLC. This article is distributed in accordance with Creative Commons Attribution Licence (http://creativecommons.org/licenses/by/4.0/).



#### Introduction

Fracture is a common clinical condition, and its healing process involves multiple cell types and complex molecular regulatory mechanisms [1]. Skeletal repair and regeneration are finely regulated biological processes that involve three stages of hematoma inflammation organization stage, primitive callus formation stage, and callus remodeling and shaping stage. The Wingless-Int-Integrated/beta-catenin (Wnt/β-catenin) signaling pathway is of utmost importance in this procedure [2,3]. Cellfate determination is controlled by the Wnt/ $\beta$ -catenin pathway in different types of cells, with a particular emphasis on its crucial involvement in osteoblast differentiation and bone-tissue formation. Recent research indicates that manipulating the function of the Wnt/ $\beta$ -catenin pathway may be a successful approach to enhancing the process of bonefracture healing [4].

As a crucial transmembrane protein, low-density lipoprotein receptor-related protein 4 (LRP4) exhibits widespread distribution across diverse cell surfaces, where it functions as an essential regulator of cellular signaling pathways [5]. In recent years, significant interest has been elicited by the role of LRP4 as a crucial controller of the Wnt/ $\beta$ -catenin signaling pathway, particularly in relation to bone metabolism [6,7]. Unlike LRP5/6, LRP4 primarily acts to inhibit Wnt signaling [8]. By binding with Wnt ligands or their co-factors, LRP4 inhibits the activation of the Wnt/ $\beta$ -catenin pathway by blocking the interaction between Wnt protein, as well as LRP5/6 [9]. In bone tissue, LRP4 expression is strictly regulated in a spatiotemporal manner, and its role in osteoblasts and osteoclasts influences the balance of bone metabolism [10]. Research has shown that the suppressive impact of LRP4 may have a vital controlling function in the stimulation of the Wnt/ $\beta$ -catenin pathway while fractures are healing [11]. Inactivating or downregulating LRP4 can enhance Wnt signal transduction, promoting osteoblast differentiation and bone-tissue formation. Thus, suppressing the function of LRP4 can offer a novel approach to stimulating the Wnt/ $\beta$ -catenin pathway and enhancing bone mending [12]. LRP4 modulates the Wnt/ $\beta$ -catenin signaling by acting as a negative regulator [6]. It can form complexes with other LRP family members and function as a decoy receptor, sequestering Wnt ligands and preventing them from binding to the LRP5/6 coreceptors. This inhibition of Wnt ligand binding leads to decreased  $\beta$ -catenin signaling activity. The suppression of LRP4 activity has been shown to enhance Wnt/ $\beta$ -catenin signaling, thereby promoting osteogenesis and improving fracture healing. In the context of fracture healing, inhibiting LRP4 can remove its suppressive effects on the Wnt/ $\beta$ catenin pathway, thereby facilitating the activation of this pathway. Enhanced Wnt/\(\beta\)-catenin signaling can promote the proliferation and differentiation of osteoprogenitor cells into mature osteoblasts, which are critical for bone regeneration and the repair process.

Alendronate is an extensively used drug for osteoporosis treatment, primarily acting by inhibiting bone resorption and increasing bone density [13]. As a bisphosphonate drug, alendronate binds to bone mineral and inhibits the activity of osteoclasts to prevent and treat osteoporosis and other bone-resorption-related diseases [14]. Alendronate inhibits enzymes in osteoclasts, particularly farnesyl pyrophosphate synthase, thereby blocking the differentiation of pre-osteoclasts and the function of mature osteoclasts, leading to osteoclast apoptosis and reduced bone resorption [15,16]. In drug delivery, nanoparticles (NPs) can improve the therapeutic effects of drugs by altering their pharmacokinetics, enhancing solubility, increasing targeting specificity, and reducing toxicity. However, alendronate-NPs may act on osteoclasts and potentially promote fracture healing by affecting the activity of osteoblasts [17,18]. The primary objective of this research was to examine the suppressive influence of alendronate-NPs on LRP4 and its consequences on fractures.

Alendronate can reportedly enhance the healing of fractures by affecting the Wnt/ $\beta$ -catenin signaling pathway [19]. Nevertheless, how it directly inhibits LRP4 and the molecular regulation of this potential impact remains unclear. In this study, ME3T3-E1 preosteoblast cells were used to gain insight into the changes in the initiation of osteoblast differentiation and various early reactions. In addition, we also established a rat fracture model. Combining these two models, we provided a theoretical basis for the key role of alendronate-NPs in the entire process of bone healing. The aim of this study was to investigate the inhibitory effect of alendronate-NPs on LRP4 and its role in promoting fracture healing by activating the Wnt/ $\beta$ -catenin signaling pathway, with the ultimate goal of advancing fracture treatment and providing additional effective therapeutic options for patients.

#### **Materials and Methods**

Alendronate-NP Preparation

NPs loaded with alendronate were synthesized by nanoprecipitation. An optimal blend of poly(lactic-coglycolic acid) (PLGA)-polyethylene glycol (PEG) and alendronate (PLGA-PEG/alendronate = 10:1) was dissolved in a blend of acetone and ethanol to form the organic phase. The aqueous phase consisted of a solution of Poloxamer 188. The organic phase was injected into the aqueous phase using a syringe while constantly stirring at 1000 rpm. The mixture was stirred at room temperature for 5 h to ensure complete evaporation of the organic solvents, resulting in the formation of alendronate@PLGA-PEG NP suspension. For the synthesis of drug-loaded mannosylated NPs, mannose was covalently adsorbed onto the particle surface through the conjugation chemistry of PLGA and carboxyl-terminated mannose (PLGA/end-carboxyl mannose = 10:1).



Particle Size and Polydispersity Index (PDI) Measurement

The physicochemical characteristics of NPs including their dimensions, uniformity (PDI), and surface charge properties were determined through dynamic light scattering analysis using a Zetasizer Nano ZS system (Malvern Panalytical Ltd., Malven, UK). Samples of NP suspensions were prepared in deionized water and, if necessary, diluted. The instrument was cleaned, and samples were loaded into the sample cell without bubbles. Measurement parameters, including sample and solvent refractive indices and viscosity, and a 10 mW HeNe laser were set with a measurement wavelength of 633 nm and a detection angle of 173° [20]. The instrument performed multiple measurements to calculate the average particle size, PDI, and zeta potential. The results were analyzed and verified for consistency.

#### Encapsulation Efficiency (EE) Determination

EE was determined using an indirect method, and the drug loading (DL) was calculated. EE was calculated using the formula: EE (%) =  $(1 - W_{free}/W_{total}) \times 100$  %. DL was calculated using the formula: DL (%) =  $(W_{total} - W_{free})/W_{NPs} \times 100$  %. Here,  $W_{free}$  represents the amount of free alendronate in the NP suspension,  $W_{total}$  is the total alendronate input, and  $W_{NPs}$  is the total mass of NPs.

#### Scanning Electron Microscopy (SEM)

The sample holder was cleaned with ethanol, and NP samples were dispersed uniformly onto the holder. Samples were fixed onto the SEM sample stage via double-sided conductive tape to ensure electrical contact. A 3  $\mu$ m gold coating was applied using a metal coater to enhance sample conductivity. Samples were examined by SEM (Quanta 200, Thermo Fisher Scientific, Waltham, MA, USA) with an accelerating voltage of 5–20 kV and a working distance of 5–10 mm. Images were captured after optimizing magnification, focus, brightness, and contrast settings for optimal visualization of NP morphology.

#### Measurement of Drug Release

Using dialysis, alendronate@PLGA-PEG NPs were placed into membranes with a molecular weight cutoff of 10 kDa and dialyzed in phosphate buffer saline (PBS) (pH 6.8 and 7.4) at 37 °C with agitation. The dialysis experiment was conducted at 100 rpm using a temperature-controlled orbital shaker (OS-300, Lab Equipment Co., Hangzhou, China). The concentration of NPs inside the dialysis bag was 1 mg/mL, with a total volume of 5 mL. The release medium outside the dialysis bag had a volume of 50 mL. At predetermined intervals, 3 mL of the release medium was collected, and an equal amount of fresh dialysis buffer was added. The alendronate concentration in the release medium was then measured using a UV-visible spectrophotometer (UV-2600, Shimadzu, Kyoto, Japan).

#### MC3T3-E1 Cell Culture

MC3T3-E1 cells (CL-0710) derived from mouse osteoblasts were acquired from Wuhan PUNOVA Life Science & Technology Co., Ltd. (Wuhan, China). cells were grown in Dulbecco's modified Eagle medium (DMEM) with 10 % fetal bovine serum (FBS) and 1 % penicillin-streptomycin (60162ES76, Yeasen, Shanghai, China) at 37 °C in a moist environment comprising 95 % air and 5 % CO<sub>2</sub>. DMEM was bought from GIBCO (12491015, Life Technologies, Rockville, MD, USA), and FBS was acquired from Merck Millipore (12103C, Billerica, MA, USA). The medium was replaced every 2 days, and cells in the exponential growth phase were utilized for subsequent experiments. MC3T3-E1 cells were divided into eight groups (control, alendronate (20  $\mu$ M), alendronate-NPs (20  $\mu$ M), alendronate-NPs (20  $\mu$ M) + OE-NC, alendronate-NPs (20  $\mu$ M) + OE-LRP4, sh-LRP4, sh-LRP4 + alendronate-NPs (20  $\mu$ M), sh-LRP4, sh-LRP4 + alendronate-NPs (20  $\mu$ M) + Nigercin) for different intervention treatments [21]. Cells were allowed to attach overnight before treatments were initiated. Medium was changed every 2–3 days during the culture period. The cell lines used in this study underwent mycoplasma testing, and they were mycoplasma free. Short tandem repeat (STR) analysis revealed that they were derived from its parental cells.

#### LRP4 Transfection

First. we treated the MC3T3-E1 cells with alendronate-NPs at a concentration of 20  $\mu$ M. Second, we transfected the treated cells with an empty vector to create the alendronate-NPs + OE-NC group, and we transfected the cells with pcDNA3.1-LRP4 to create the alendronate-NPs + OE-LRP4 group. cells were transfected with negative control to LRP4 shRNA and LRP4 short hairpin RNA (shRNA), and sh-NC and sh-LRP4 groups were established. MC3T3-E1 cells were transfected with the pcDNA3.1 empty vector (pcDNA-null), pcDNA3.1-LRP4 overexpression vector (5'-TGCCCACCACCTTACATTCT-3' and 5'-GAACTGCTTCCTTCACGACAT-3'), tive control to LRP4 shRNA and LRP4 shRNA (5'-GATCCCGGAAGTTTCCTGACATAAATTCAAGAGAT TTATGTCAGGAAACTTCCTTTTTGGAAA-3' and 5'-AGCTTTTCCAAAAAGGAAGTTTCCTGACATAAATC TCTTGAATTTATGTCAGGAAACTTCCGG-3') by using Lipofectamine 2000 (11668027, Thermo Fisher Scientific, Wilmington, MA, USA). Samples were obtained 24 h after transfection for future investigations. The pcDNA3.1 empty vector (pcDNA-null) and the pcDNA3.1-LRP4 overexpression vector (pcDNA-LRP4) were constructed by Shanghai Jima Pharmaceutical Technology Co., Ltd. (Shanghai, China).



#### TUNEL Assay

We prepared  $1 \times 10^4$  cells/well on glass coverslips in 24-well plates. MC3T3-E1 cells treated with alendronate or alendronate-NPs were cultured for 72 h. Fixed MC3T3-E1 cells were prepared on glass slides. The terminal deoxynucleotidyl transferase-mediated dUTP nick end labeling (TUNEL) reaction mixture (T2191, Solarbio, Beijing, China) was prepared according to the manufacturer's instructions. The TUNEL reaction mixture was applied to the MC3T3-E1 cells, ensuring that all samples were adequately covered. The samples were incubated at 37 °C in a dark environment for 2 h. After incubation, they were washed with wash buffer. For samples on glass slides, 4',6-diamidino-2-phenylindole (DAPI) (C1005, Thermo Fisher Scientific, Waltham, MA, USA) mounting medium was added for fixation. The samples were examined under a fluorescence microscope (BX51FL, Olympus Corporation, Tokyo, Japan). Subsequently, TUNEL-positive cells were counted to quantify the level of apoptosis in the samples.

#### EdU Assav

At a density of  $1\times10^5$  cells/mL, a 100  $\mu$ L cell suspension was added into each 96-well plate. An EdU cell-proliferation kit (CA1170, Solarbio, Beijing, China) was used, and 100  $\mu$ L EdU solution was added to each well. Then, 50  $\mu$ L of 4 % paraformaldehyde (P0099, Beyotime Biotechnology, Shanghai, China) was added to fix the cells for 30 min. Finally, a PBS solution (C0221A, Beyotime Biotechnology, Shanghai, China) of 0.6 % Triton X-100 (T8200, Solarbio, Beijing, China) was used and incubated for 15 min. The images were observed by fluorescence microscope.

#### Transwell Assay

We placed  $1\times10^5$  cells into the upper cavity of a 24-well plate with a pore size of 8  $\mu m$  and added 15 % FBS into the lower cavity medium. After incubation at 37 °C for 48 h, cells were fixed with 4 % paraformaldehyde for 15 min and stained with 0.1 % crystal violet (BL2247A, Biosharp, Hefei, China) for 30 min. For the invasion experiment, the upper cavity was pre-coated with 100  $\mu L$  diluted Matrigel. Finally, an inverted microscope was used to observe and capture images.

#### Cellular Uptake Assay

The cells were inoculated on 12-well plates (2  $\times$   $10^4$  cells/well) and incubated overnight. Then, 100  $\mu L$  of 1 mg/mL TITC-labeled alendronate-NPs was added onto a 12-well plate and incubated at 37 °C for 2 h. The cells were washed twice with PBS, and the nuclei were stained with DAPI.

Table 1. Primer sequences used in this study.

Primes name	Primes sequences (5′–3′)
PCNA-F	AGGGTTGGTAGTTGTCGCTG
PCNA-R	ATTCACCCGACGGCATCTTT
Runx2-F	ACTTCGCTAACTTGTGGCTGT
Runx2-R	GGATGAGGAATGCGCCCTAA
OCN-F	GAACAGACAAGTCCCACACAGC
OCN-R	TCAGCAGAGTGAGCAGAAAGAT
LRP4-F	GCCAAGCTCACAGAGACGAT
LRP4-R	CCTGAGAACAATCCCTGCCT
Wnt4-F	CCCTCGCAGTTTTGTCCTCT
Wnt4-R	CATGGGAGCCACTTGGACAT
GSK-3 $\beta$ -F	AGGAACACCAACAAGGGAGC
GSK-3 $\beta$ -R	TCCTGGGGTGAAATGTCCTG
GAPDH-F	TGTCTCCTGCGACTTCAACA
GAPDH-R	GGTGGTCCAGGGTTTCTTACT

PCNA, proliferating cell nuclear antigen; Runx2, runt-related transcription factor 2; OCN, osteocalcin; LRP4, lipoprotein receptor-related protein 4; Wnt4, Wingless-type MMTV integration site family, member 4; GSK-3 $\beta$ , glycogen synthase kinase 3 beta; GAPDH, glyceraldehyde 3-phosphate dehydrogenase.

# Quantitative Reverse-Transcription (qRT) Polymerase Chain Reaction (PCR)

Total RNA was extracted from the samples of cells cultured for 48 h using an RNA extraction kit (15596026, Thermo Fisher Scientific, Wilmington, MA, USA). The extracted RNA was reverse transcribed into complementary DNA (cDNA) using a cDNA reverse transcription kit (RR390A, Takara Bio, Tokyo, Japan). The synthesized cDNA was amplified to ensure sufficient quantity for subsequent PCR amplification. Primers were designed for amplification in specific regions of the target gene. First, initial denaturation was performed at 95 °C for 2 Second, we performed the cycling steps, which included denaturation (95 °C for 30 s), annealing (55 °C for 30 s), and extension (72 °C for 2 min), for a total of 30 cycles. After the cycles, a final extension was performed at 72 °C for 5 min. Finally, the PCR products were held at 4 °C for temporary storage. Glyceraldehyde 3-phosphate dehydrogenase (GAPDH) was selected as the reference gene. The relative expression was calculated using the following formula: relative expression 2(-((CT target - CT GAPDH) sample - (CT target - CT GAPDH) control)) The primer sequences used in this study are listed in Table

# Cell Counting Kit-8 (CCK-8) Assay for MC3T3-E1 Cell Proliferation

The manufacturer's instructions were followed to seed transfected cells (5  $\times$  10<sup>3</sup> cells/well) onto a 96-well plate. Following 24, 48, and 72 h of incubation, the medium was extracted, and 100  $\mu$ L of complete DMEM supplemented



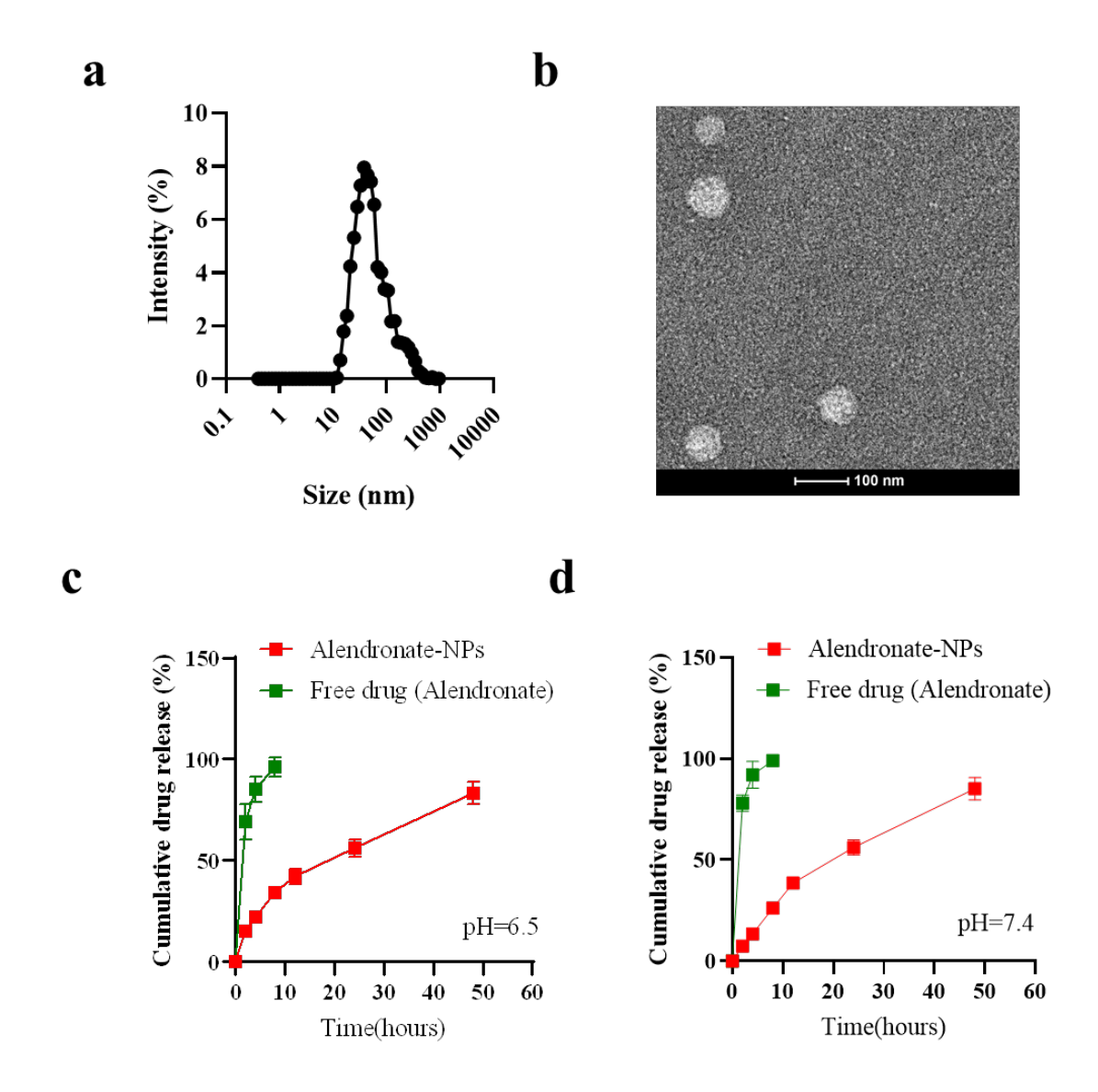


**Fig. 1.** Characterization of Physicochemical Properties of Alendronate@PLGA-PEG NPs. Size-distribution chart (a) and scanning electron microscopy image (b) of alendronate@PLGA-PEG NPs. Scale bar = 100 nm. (c,d) Release curves of alendronate in free drug and from PLGA-PEG in solution (pH 6.5 and 7.4). NPs, nanoparticles; PLGA, poly(lactic-co-glycolic acid); PEG, polyethylene glycol. The images were plotted using GraphPad Prism 8.0 software.

with 10 % CCK-8 solution (CA1210, Solarbio, Beijing, China) was introduced into each well under low light conditions. After incubating the plate at 37 °C for 4 h, the culture was subsequently stopped. A shaker was used to shake the plate for 5 min at ambient temperature, and a microplate reader (Multiskan<sup>TM</sup> FC, Thermo Fisher Scientific, Waltham, MA, USA) was utilized to measure the absorbance at a wavelength of 450 nm. Three trials were conducted.

# Western Blot Analysis of Protein Expression

About  $2 \times 10^5$  cells/well in 6-well plates were cultured for 48 h, collected, and lysed in radioimmunoprecipitation assay (RIPA) lysis buffer on ice. The bicinchoninic acid assay (BCA) method was used to determine the pro-

tein concentration in the cells and tissues. A 10 % sodium dodecyl sulfate polyacrylamide gel electrophoresis (SDS-PAGE) gel was used to separate 50  $\mu$ g of protein samples, followed by transferring the proteins onto a polyvinylidene fluoride (PVDF) membrane at 80 V for 30 min and 120 V for 90 min. The wet transfer method was conducted using Bio-Rad Trans-Blot Cell. The transfer conditions were as follows: 100 V for 90 min at 4 °C. After blocking the PVDF membrane (IPVH00010, Millipore Corporation, Billerica, MA, USA) with 5 % non-fat milk, primary antibodies (Abcam, Cambridge, MA, USA) against LRP4 (ab230188, 1:1000), Wingless-type MMTV integration site family, member 4 (Wnt4) (ab262696, 1:1000), glycogen synthase kinase 3 beta (GSK3 $\beta$ ) (ab227208, 1:1000), p-GSK3 $\beta$  (ab68476, 1:1000),  $\beta$ -catenin (ab68183, 1:1000),



and GAPDH (ab8245, 1:2000) were added and incubated overnight at 4 °C. The next day, horseradish peroxidase (HRP)-conjugated secondary antibodies were added and incubated at room temperature for 2 h. This study used the HRP-conjugated affinity goat anti-rabbit immunoglobulin G (IgG) (H + L) secondary antibody (PR30012, 1:1000, Proteintech Group, Wuhan, China). Enhanced chemiluminescence reagent (P0018S, Beyotime, Shanghai, China) was used for visualization via a gel-imaging system (ChemiDoc MP, Bio-Rad, Hulsey, CA, USA). Image J software (version 2.x, National Institutes of Health, Bethesda, MD, USA) was used for analysis.

#### Assay for Alkaline Phosphatase (ALP) Activity

First, we prepared 1 M diethanolamine buffer (pH 9.8) and 1 M MgCl<sub>2</sub> solution. For the substrate solution, we used freshly prepared 10 mM pNPP solution. We added 80  $\mu \rm L$  of buffer and 20  $\mu \rm L$  of substrate solution onto each well of a 96-well plate, followed by 20  $\mu \rm L$  of sample or blank control. The plate was incubated at 37 °C for 30–60 min and added with 50  $\mu \rm L$  of 0.1 M NaOH to stop the reaction. Finally, the absorbance was measured using a microplate reader, and ALP activity was calculated based on a standard curve or calculation formula.

#### Alizarin Red Staining

We subjected  $2 \times 10^4$  cells/well of 24-well plates to various treatments. They were initially fixed and subsequently stained using a 1 % solution of alizarin red (60504ES, Yeasen, Shanghai, China) for 20 min. An optical microscope (CX41-32RFL, Olympus, Tokyo, Japan) was used to capture images of five distinct and unrelated regions at a magnification of 200×. The quantification method involved analyzing five random fields per well at 200× magnification using Image J software (v1.8.0.345, National Institutes of Health, Bethesda, MD, USA). The process included converting images to 8-bit grayscale, setting a threshold to identify positively stained areas, measuring the total and stained areas, and calculating the percentage using the following formula: % stained area = (stained area/total area) × 100 %. The high percentage values in alendronate-NPs samples reflected the dense mineralization nodules formed in these cultures.

# Rat Fracture Animal Model

A total of 24 Sprague-Dawley rats were obtained from Jinan Pengyue Experimental animal Breeding Co., Ltd. (Jinan, China). The subjects were adult male rats, aged 8 weeks, with a body weight of 250–300 g. The rats were kept in a controlled environment within a temperature range of 21 °C–23 °C and a 12 h light/dark cycle to mimic natural day and night cycles. They were provided with unlimited access to food and water. Surgical methods refer to previous reports [22,23]. The rats were anesthetized by intraperitoneal injection of 1 % pentobarbital sodium (45 mg/kg,

Shandong Xiya Chemical Industry Co., Ltd., Linyi, China). The left tibia of the rats was routinely shaved, and the tibia was cut down about 1.5 cm from the tibial tubercle to expose the tibia. The middle and lower one-third of the tibia was cut laterally with bone scissors, and the wound was disinfected and closed layer by layer. Notably, the periosteum of the tibia was preserved as much as possible. The blood was washed with saline and coated with iodophor, and 0.1 mL of gentamicin was injected to prevent wound infection. The tibial fracture was then externally immobilization with a small splint, which was wrapped in selfadhesive tape and kept in a separate cage. The success rate of fracture modeling in rats was 75 %. The 24 rats were randomly divided into four groups with 6 rats each (control group, model group, alendronate group, and alendronate-NP group). The remaining six unoperated rats served as a control group. Alendronate or alendronate-NP rats were given 50 mg/kg of alendronate or alendronate-NPs orally once a day for 7 days [24]. After 7 days of treatment with alendronate, the rats were euthanized with 100 mg/kg pentobarbital, and tibia tissue was collected from the fracture site along with venous blood.

#### Staining of Hematoxylin-Eosin (HE) in Tissue

HE staining was performed with kit (C0115S, Beyotime Biotechnology, Shanghai, China). Before analysis, soft tissue was carefully removed while preserving the callus formation. First, we placed the bone tissue in 10 % ethylenediaminetetraacetic acid (EDTA, 60126ES, Yeasen, Shanghai, China) solution at room temperature or 4 °C, changing the solution daily for decalcification. The decalcification process lasted for 2-4 weeks, depending on the size and hardness of the sample. Second, we dehydrated the tissue using a gradient ethanol series (70 %, 95 %, and 100 %) for 2-5 min each step and cleared with xylene for 5 min per step. This step was repeated 2-3 times, followed by embedding the sample in paraffin. After sectioning 5–7  $\mu$ m-thick slices, the slices were deparaffinized with xylene for 5–10 min per step, which was repeated 2–3 times. Thereafter, the slices were rehydrated through a gradient ethanol series (100 %, 95 %, 70 %, 50 %, and distilled water) for 2–5 min each step. The sections were stained with hematoxylin solution for 5–10 min, differentiated in 1 % hydrochloric acid ethanol (1 % HCl in 70 % ethanol) for a few seconds to 1 min and rinsed with tap water or ammonia water for a few minutes. After staining with 0.5 %–1 % eosin solution for 1-3 min, the sections were dehydrated again through a gradient ethanol series (70 %, 95 %, and 100 %) for 2-5 min each step, cleared with xylene for 5 min per step, repeated twice, and finally mounted with neutral gum. The prepared sections were observed and photographed under a light microscope (DM750, Leica Microsystems, Wetzlar, Hesse, Germany) to examine the tibiae fracture end tissue.



#### *Immunohistochemistry*

For protein detection and localization, tissue specimens were processed through standard immunohistochemical protocols. In a typical procedure, tissue sections underwent sequential processing, including deparaffinization and gradient alcohol rehydration. Following heat-mediated epitope retrieval in citric buffer solution, endogenous peroxidase was neutralized, and non-specific binding sites were masked with bovine serum albumin (BSA) solution. The processed sections were probed with collagen I-specific primary antibody (4 °C, overnight incubation, 1:200; #72026, CST, Boston, MA, USA), followed by HRP-linked secondary antibody (1:1000; #7074, CST, Boston, MA, USA) treatment. Protein expression was revealed by diaminobenzidin (DAB) chromogenic reaction, yielding characteristic brown deposits. Nuclei were visualized through hematoxylin counterstaining, followed by standard dehydration and mounting procedures. For collagen I quantification, we analyzed five independent biological samples per group (n = 5). From each sample, five random non-overlapping fields were captured at 200× magnification. The intensity of collagen I immunostaining was quantified using Image J software by measuring the integrated optical density (IOD) of the positive staining area. The results were expressed as the mean IOD  $\pm$  SD.

#### ALP Activity Measurement

For serum ALP activity analysis, blood samples were collected after treatment and centrifuged to obtain serum. For cell culture ALP activity, MC3T3-E1 cells were seeded onto 24-well plates and lysed with 0.2 % Triton X-100 after treatment, followed by centrifugation at 12,000 g for 10 min. ALP activity was measured using a reaction mixture containing 80  $\mu$ L of diethanolamine buffer (1 M, pH 9.8), 20  $\mu$ L of pNPP substrate solution (10 mM), and 20  $\mu$ L of sample or blank control. The mixture was incubated at 37 °C for 30–60 min, and the reaction was stopped by adding 50  $\mu$ L of 0.1 M NaOH. The absorbance was measured at 405 nm using a Multiska TM FC microplate reader. For cell-culture samples, results were normalized to total protein content determined by BCA assay. All measurements were performed in triplicate.

#### Statistical Analysis

Statistical analysis was conducted utilizing the statistical software SPSS 22. 0 (IBM Corporation, Armonk, NY, USA). The data were displayed as the average plus the standard deviation. T-tests were utilized to analyze the variances between two groups. Differences among multiple groups were analyzed using one-way Analysis of Variance (ANOVA) and Tukey's post hoc test (HSD). Statistical significance was attributed to a significance level lower than 0.05, denoted as p < 0.05.

Table 2. Physicochemical property parameters of nanoparticles.

Parameters	Alendronate@PLGA-PEG NPs
EE (%)	$64.02 \pm 0.73$
DL (%)	$32.14 \pm 0.52$
Particle size (nm)	$128.33 \pm 5.34$
PDI	$0.12 \pm 0.01$
Zeta (mV)	$-17.25 \pm 0.05$

PDI, polydispersity index; EE, encapsulation efficiency; DL, drug loading; NPs, nanoparticles; PLGA, poly(lactic-co-glycolic acid); PEG, polyethylene glycol.

#### Results

Characterization of Physicochemical Properties of Alendronate@PLGA-PEG NPs

As presented in Table 2 and depicted in Fig. 1, the alendronate@PLGA-PEG NPs exhibited a particle size of  $128.33 \pm 5.34$  nm, an EE of 64.02 %  $\pm 0.73$  %, a drug payload of 32.14 %  $\pm$  0.52 %, and a PDI of 0.12  $\pm$  0.01; they carried a negative charge with a potential of -17.25  $\pm$  0.05 mV. The NP size-distribution chart and SEM image of alendronate@PLGA-PEG NPs are shown in Fig. 1. Additionally, we investigated the drug-release profiles of alendronate@PLGA-PEG NPs and free drug under different pH conditions. As shown in Fig. 1c,d, the cumulative release of alendronate@PLGA-PEG NPs reached over 80 % within 48 h in pH 6.5 solution. Similar release patterns were observed in pH 7.4 solution. Conversely, the free drug exhibited rapid and complete release within a short period. These results demonstrated the sustained-release properties of alendronate@PLGA-PEG NPs.

#### Cellular Uptake of Alendronate-NPs

Fig. 2a,b shows the uptake of alendronate-NPs by MC3T3-E1 cells at 2, 4, and 6 h. Results showed that the uptake capacity of alendronate-NPs increased gradually with increased time (p < 0.001).

Alendronate-NPs can Promote Calcium Deposition and Differentiation into Osteoblasts in MC3T3-E1 Cells

The alendronate treatment group exhibited a notably greater intensity of alizarin red S staining than the control group. This result suggested that the administration of alendronate may enhance calcium deposition in osteoblasts. The experimental results demonstrated a significant increase in calcium deposition in osteoblasts in the alendronate treatment group. The phenomenon of calcium deposition in osteoblasts was more pronounced in the alendronate-NPs group (Fig. 3a,b). These findings provided important experimental support for the role of sodium alendronate in promoting fracture-healing mechanisms. Cell activity was higher in the alendronate-NP treatment group than in the alendronate treatment group (p < 0.05). Additionally, we assessed the influence of al-



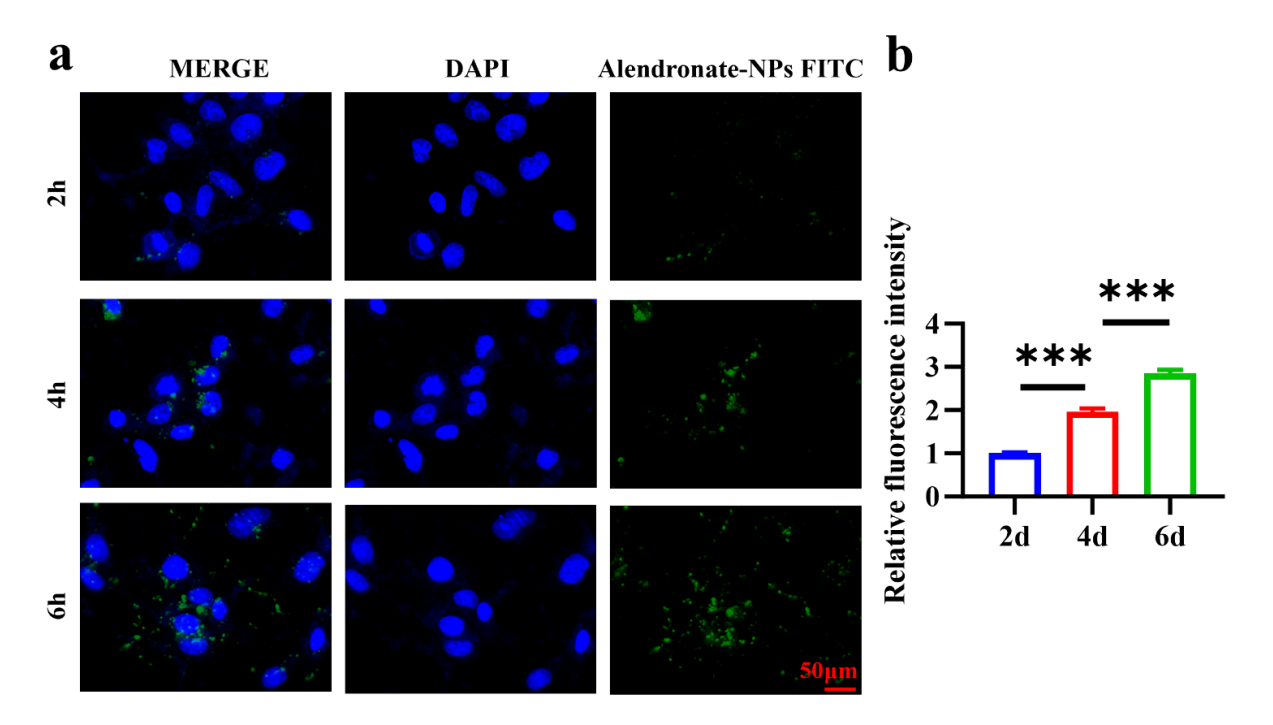


Fig. 2. Cellular uptake of different nanoparticles. (a) Fluorescence image of MC3T3-E1 cells incubated with alendronate-NPs for 2 h. Scale bar = 50  $\mu$ m. (b) Quantification of the relative fluorescent intensity of MC3T3-E1 cells incubated with alendronate-NPs for 2 h. DAPI, 4',6-diamidino-2-phenylindole; FITC, fluorescein isothiocyanate isomer. N = 3. \*\*\*p < 0.001. The images were plotted using GraphPad Prism 8.0 software.

endronate on the differentiation of MC3T3-E1 cells into bone cells by examining the levels of proliferating cell nuclear antigen (PCNA), runt-related transcription factor 2 (Runx2), osteocalcin (OCN), and osteopontin (OPN) proteins. Compared with the control group, the sodium alendronate treatment group or alendronate-NP group exhibited elevated expression levels of PCNA and Runx2. The expression levels of OCN and OPN also increased (p < 0.01). Changes in the levels of these proteins were more significant in the alendronate-NP group than in the alendronate group (p < 0.05; Fig. 3c,d). These findings suggested that alendronate may enhance the osteogenic differentiation of MC3T3-E1 cells by potentially activating the Wnt/βcatenin pathway. The qRT-PCR results revealed that alendronate treatment or alendronate-NP treatment significantly increased the messenger ribonucleic acid (mRNA) levels of PCNA, Runx2, OCN, and OPN compared with the control group (p < 0.01). These changes became significant after alendronate-NPs treatment (p < 0.05 and p < 0.01; Fig. 3e-h).

Alendronate Promoted Cell Activity, Inhibiting Apoptosis

The proliferation of MC3T3-E1 cells was evaluated by CCK-8 assay to determine the influence of alendronate. The experimental results showed that the growth rate of MC3T3-E1 cells in the group treated with alendronate or alendronate-NPs was considerably greater than that in the control group. This finding indicated that alendronate

can enhance the proliferation of MC3T3-E1 cells (p < 0.01) (Fig. 4a). Compared with the control group, alendronate alone treatment and alendronate-NPs treatment significantly enhanced ALP activity in osteoblasts (p < 0.01 and p < 0.001). However, the enhancement in ALP activity was more pronounced following treatment with alendronate-NPs than with alendronate alone (Fig. 4b). Additionally, the TUNEL staining results of MC3T3-E1 cells demonstrated a significant decrease in TUNEL staining intensity following alendronate treatment compared with the control group (p < 0.001). Compared with the alendronate group, the TUNEL staining intensity significantly decreased after treatment with alendronate-NPs (p < 0.01; Fig. 4c,d).

By Targeting LRP4, Alendronate Triggered the Activation of the Wnt/\beta-Catenin Signaling Pathway

The alendronate treatment group and alendronate-NPs treatment showed a notable decrease in LRP4 expression in cells (p < 0.01 and p < 0.001). The changes were more pronounced with alendronate-NPs treatment than with alendronate alone. This finding indicated that the effects of alendronate may be achieved through LRP4 inhibition. The alendronate treatment group and alendronate-NPs treatment group showed a significant increase in Wnt4 expression (p < 0.01), suggesting that treatment with alendronate can trigger the activation of the Wnt/ $\beta$ -catenin signaling pathway. The expression of GSK-3 $\beta$  was not signaling pathway.



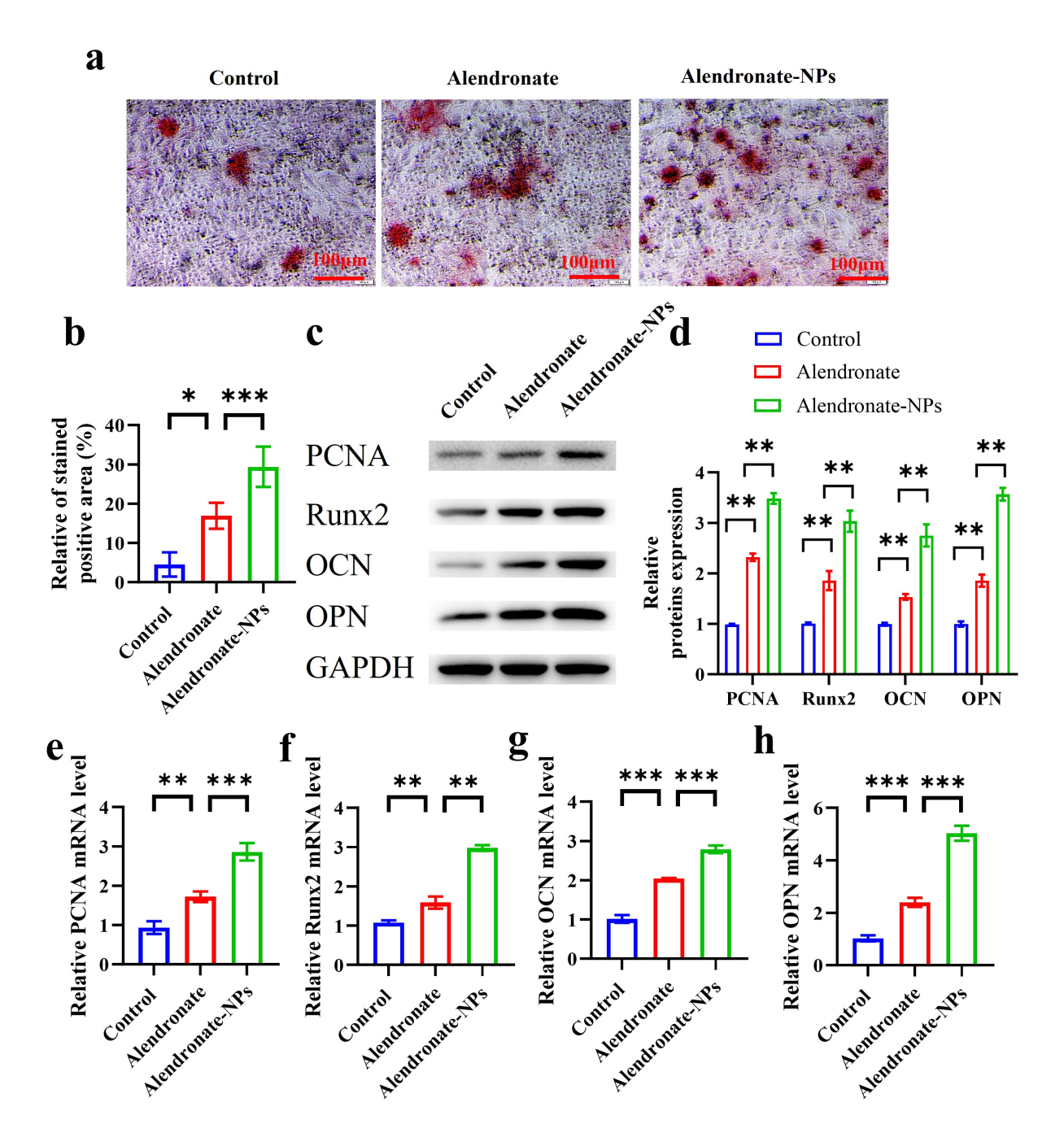


Fig. 3. Alendronate-NPs can promote calcium deposition and differentiation into osteoblasts in MC3T3-E1 cells. (a) Alizarin red S staining results. Scale bar =  $100 \ \mu m$ . (b,c) Expression of PCNA, Runx2, OCN, and OPN proteins in alendronate-treated MC3T3-E1 cells analyzed by Western blot. (d-h) Analysis of *PCNA*, *Runx2*, *OCN*, and *OPN* gene expression in MC3T3-E1 cells treated with alendronate using qRT-PCR. \*p < 0.05, \*\*p < 0.01, and \*\*\*p < 0.001. N = 3. PCNA, proliferating cell nuclear antigen; Runx2, runt-related transcription factor 2; OCN, osteocalcin; OPN, osteopontin; qRT, quantitative dlreverse-transcription; PCR, polymerase chain reaction; GAPDH, glyceraldehyde 3-phosphate dehydrogenase; mRNA, messenger ribonucleic acid. The images were plotted using GraphPad Prism 8.0 software.

nificantly affected by alendronate treatment or alendronate-NPs treatment. However, the expression of p-GSK3 $\beta$  significantly increased in the alendronate treatment group and alendronate-NPs treatment group (p < 0.01), suggesting that alendronate treatment can activate p-GSK3 $\beta$ . The  $\beta$ -

catenin expression level exhibited a significant increase in the group treated with alendronate (p < 0.01), providing further evidence for the activation of the Wnt/ $\beta$ -catenin signaling pathway by alendronate or alendronate-NPs (Fig. 5a,b). Furthermore, qRT-PCR results indicated that com-

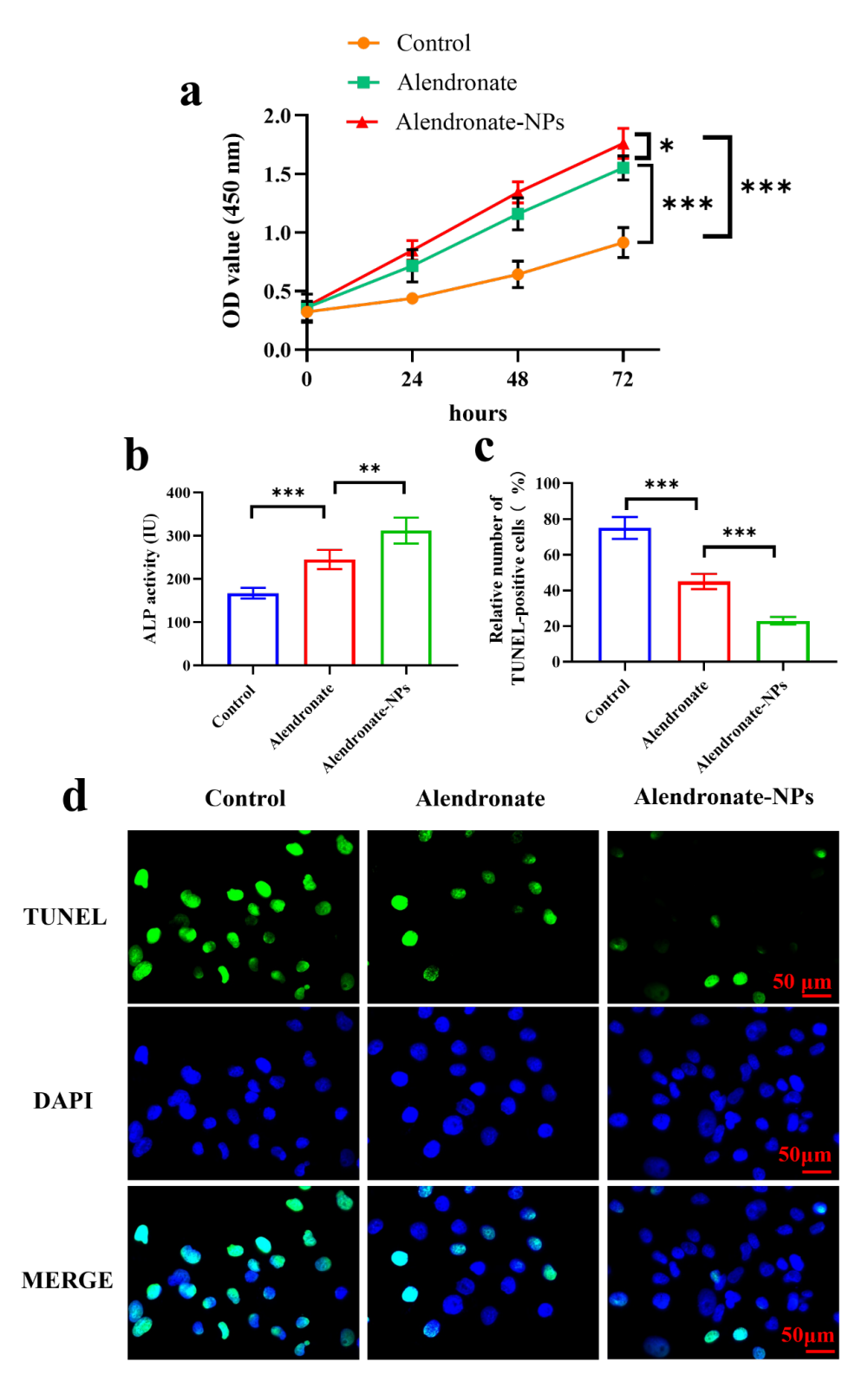


Fig. 4. Alendronate promotes cell activity, inhibiting apoptosis. (a) CCK-8 assay was used to evaluate the growth rate of MC3T3-E1 cells treated with alendronate. (b) Determination of ALP activity in osteoblasts. (c,d) TUNEL staining of the MC3T3-E1 cells and quantitative analysis. Scale bar = 50  $\mu$ m. N = 3. \*p < 0.05, \*\*p < 0.01, \*\*\*p < 0.001. CCK-8, cell counting kit-8; ALP, alkaline phosphatase; TUNEL, terminal deoxynucleotidyl transferase-mediated dUTP nick end labeling; OD, optical delnsity. The images were plotted using GraphPad Prism 8.0 software.



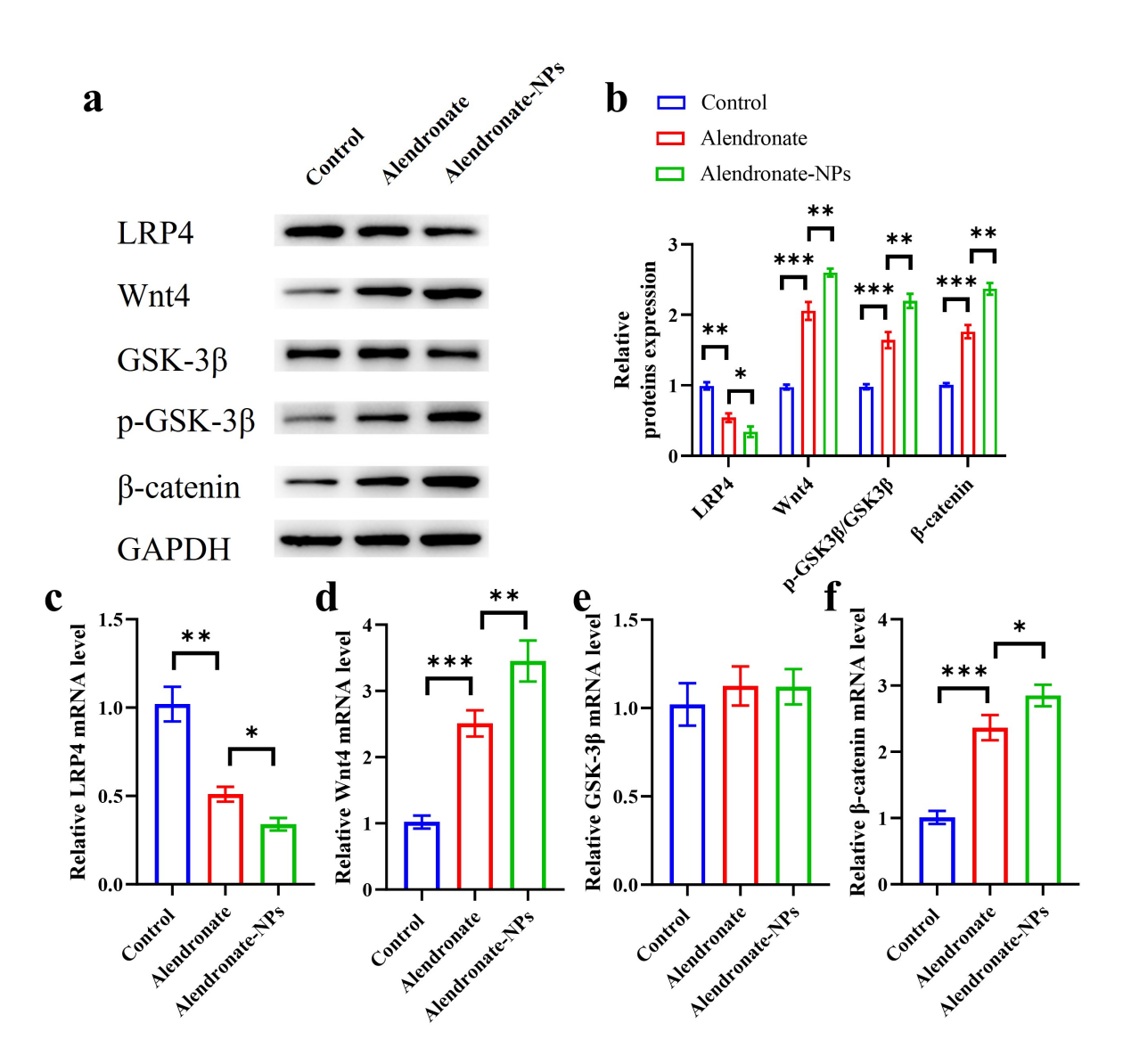


Fig. 5. By targeting LRP4, alendronate triggers the activation of the Wnt/ $\beta$ -catenin signaling pathway. (a,b) The impact of alendronate on the protein expression of LRP4 and the Wnt/ $\beta$ -catenin pathway in MC3T3-E1 cells was examined by Western blot analysis. (c-f) The effects of alendronate on the mRNA expression of LRP4 and the Wnt/ $\beta$ -catenin pathway in MC3T3-E1 cells were assessed through qRT-PCR analysis. The value of p is less than 0.01. N = 3. \*p < 0.05, \*\*p < 0.01, and \*\*\*p < 0.001. LRP4, lipoprotein receptor-related protein 4; Wnt4, Wingless-type MMTV integration site family, member 4;  $\beta$ -catenin, beta-catenin; GSK-3 $\beta$ , glycogen synthase kinase 3 beta. The images were plotted using GraphPad Prism 8.0 software.

pared with the control group, alendronate or alendronate-NPs treatment significantly increased the mRNA levels of Wnt4 and  $\beta$ -catenin but decreased the mRNA level of LRP4 (p < 0.01; Fig. 5**c**-**f**). However, it did not affect the mRNA level of GSK-3 $\beta$  (Fig. 5**c**-**f**). Compared with the alendronate treatment group, changes in the alendronate-NPs treatment group were more significant. In summary, our experimental findings suggested that alendronate facilitated the mending of fractures by suppressing LRP4 and triggering the Wnt/ $\beta$ -catenin signaling pathway.

Alendronate-NP Promotion of Proliferation and Osteogenic Differentiation was Reversed by LRP4 Overexpression

The control group exhibited a high expression level of LRP4 protein in cells, whereas the alendronate-NPs treatment group with OE-NC showed a low expression (p < 0.01; Fig. 6a,b). In the alendronate-NPs treatment + OE-LRP4 group, the expression level of LRP4 increased again (p < 0.01; Fig. 6a,b). This result suggested that the use of alendronate-NPs can suppress LRP4 expression. The expression of GSK3 $\beta$  did not show significant changes in all groups, suggesting that the influence of alendronate-NPs on GSK3 $\beta$  may be minimal. However, the level of



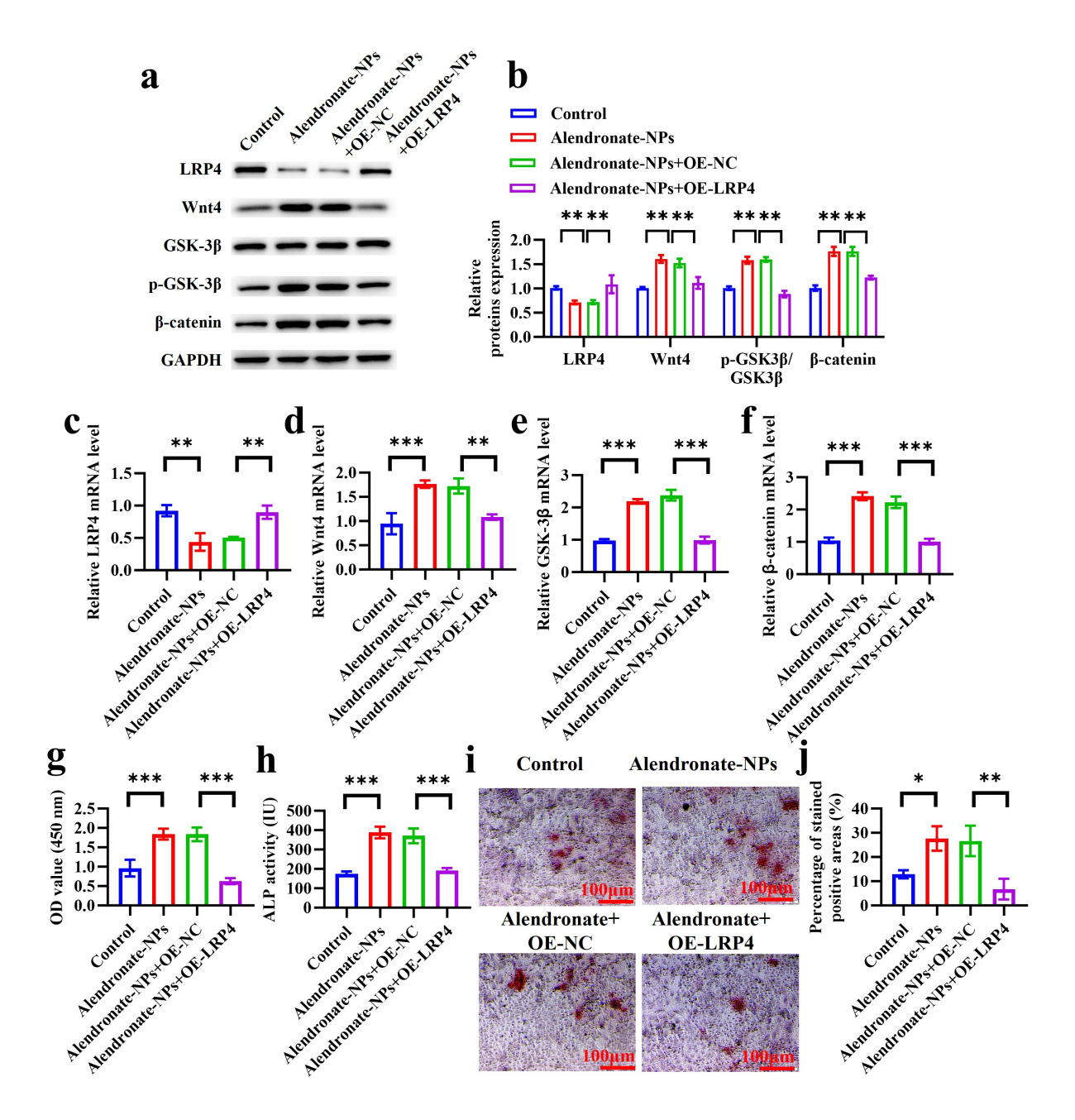


Fig. 6. LRP4 overexpression reverses the promotion of proliferation and osteogenic differentiation by sodium alendronate. (a,b) Effect of sodium alendronate on the expression of LRP4 and Wnt/ $\beta$ -catenin pathway-related proteins in MC3T3-E1 cells analyzed by Western blot. (c-f) Impact of alendronate on the expression of LRP4 and genes associated with the Wnt/ $\beta$ -catenin pathway in MC3T3-E1 cells through qRT-PCR. (g) Proliferation rate of MC3T3-E1 cells assessed by CCK-8 assay. (h) ALP activity. (i,j) Alizarin red S staining results. Scale bar =  $100 \ \mu \text{m}$ . \*p < 0.05, \*\*p < 0.01, \*\*\*p < 0.001. N = 3. The images were plotted using GraphPad Prism 8.0 software.

p-GSK3 $\beta$ /GSK3 $\beta$  increased in the alendronate-NP treatment group (p < 0.01). Following LRP4 overexpression, the p-GSK3 $\beta$ /GSK3 $\beta$  level declined (p < 0.01). In the alendronate-NPs + OE-NC group,  $\beta$ -catenin expression notably increased, whereas the alendronate-NPs + OE-LRP4 group experienced a decrease in this expression (p < 0.01). Thus, alendronate-NPs treatment can activate  $\beta$ -catenin, and LRP4 overexpression may reverse this activation effect (Fig. 6a,b). qRT-PCR results further demonstrated that

compared with the control group, alendronate-NPs + OE-NC treatment significantly increased the mRNA levels of Wnt4 and  $\beta$ -catenin but decreased the mRNA level of LRP4 (p < 0.01; Fig. 6c–f). However, it did not affect the mRNA level of GSK-3 $\beta$ . Compared with the alendronate-NPs + OE-NC group, alendronate-NPs + OE-LRP4 treatment significantly elevated the mRNA level of LRP4 and reduced the mRNA levels of Wnt4 and  $\beta$ -catenin (p < 0.01), but it had no impact on the mRNA level of GSK-3 $\beta$  (Fig. 6c–f).



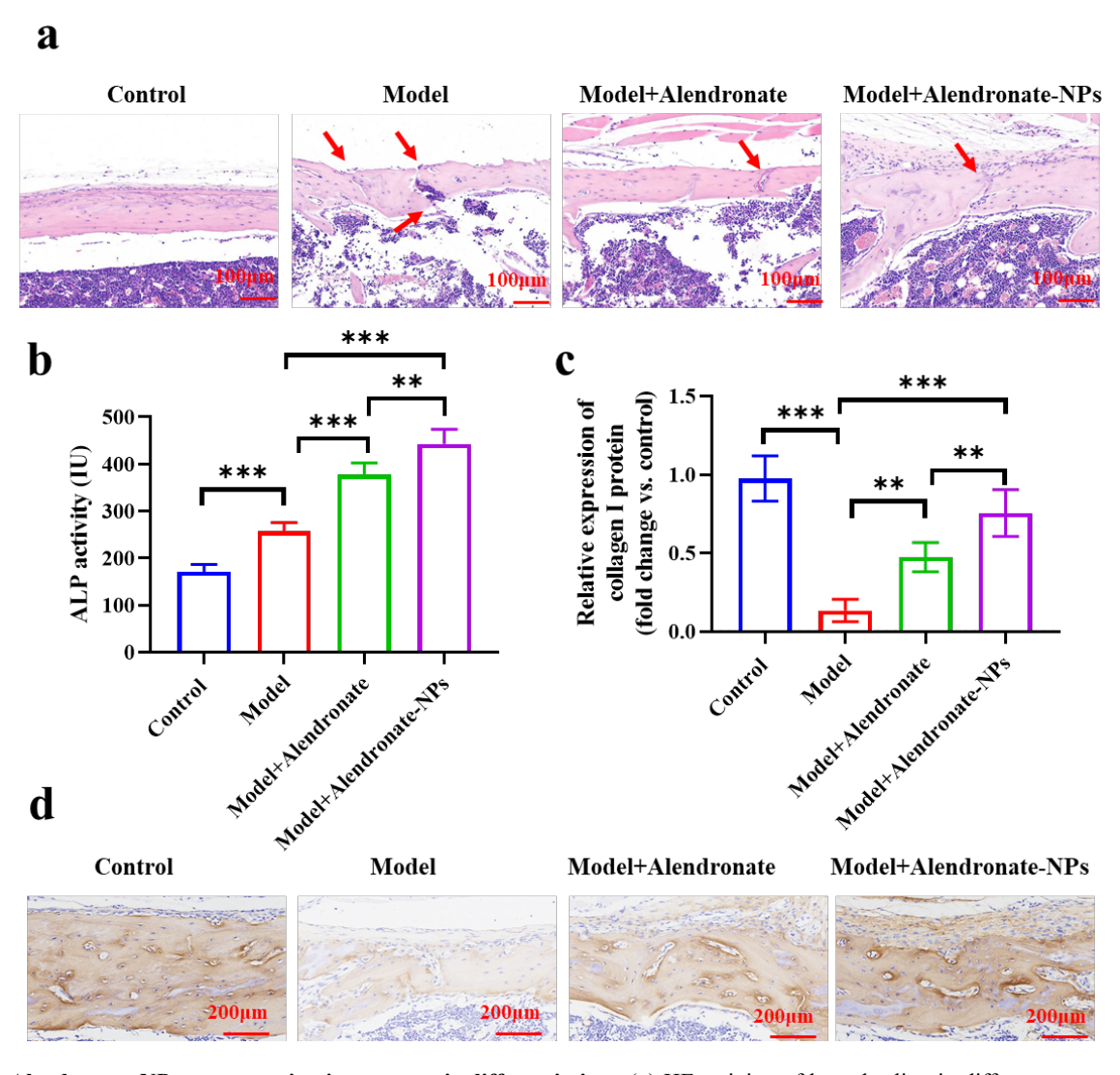


Fig. 7. Alendronate-NPs promotes *in vivo* osteogenic differentiation. (a) HE staining of bone healing in different groups of rats. Red arrows represent fracture healing. Scale bar =  $100 \mu m$ . (b) ALP activity in the serum of rats in various groups was detected using a microplate technique involving p-nitrophenyl phosphate. (c,d) Immunohistochemical picture and quantitative analysis of collagen. Scale bar =  $200 \mu m$ . N = 5. \*\*p < 0.01, and \*\*\*p < 0.001. HE, hematoxylin-eosin. The images were plotted using GraphPad Prism 8.0 software.

CCK-8 assay results revealed that the group treated with alendronate-NPs + OE-LRP4 had the lowest cell proliferation rate, whereas the alendronate-NPs + OE-NC group showed a slightly lower rate than the control group (p < 0.01). Thus, LRP4 overexpression can reverse the promoting effect of alendronate-NPs on cell proliferation (Fig. 6g). Results further showed that ALP activity in the alendronate-NPs group significantly increased compared with the control (p < 0.01). Compared with the alendronate-NPs+OE-NC group, ALP activity in the alendronate-NP + OE-LRP4 group significantly decreased (p < 0.01; Fig. 6h). Thus, LRP4 overexpression can reverse the promoting effect of alendronate-NPs on osteogenic differentiation (Fig. 6h). The staining results of alizarin red S indicated that the intensity of staining with alizarin red was the least in the group

treated with alendronate-NPs + OE-LRP4, followed by the control group, and the highest intensity was observed in the group treated with alendronate-NPs + OE-NC. Therefore, LRP4 overexpression can reverse the promoting effect of alendronate-NPs on osteogenic differentiation (Fig. 6i,j).

# Alendronate-NPs Promoted In Vivo Osteogenic Differentiation

To examine fracture healing, we initially established an animal model for fractures to study the mechanism of action of alendronate. To examine the morphology and structure of tissues, we performed HE staining. In this experiment, HE staining was used to assess the bonehealing status in each group of rats and determine the effect of alendronate on bone healing. In the model



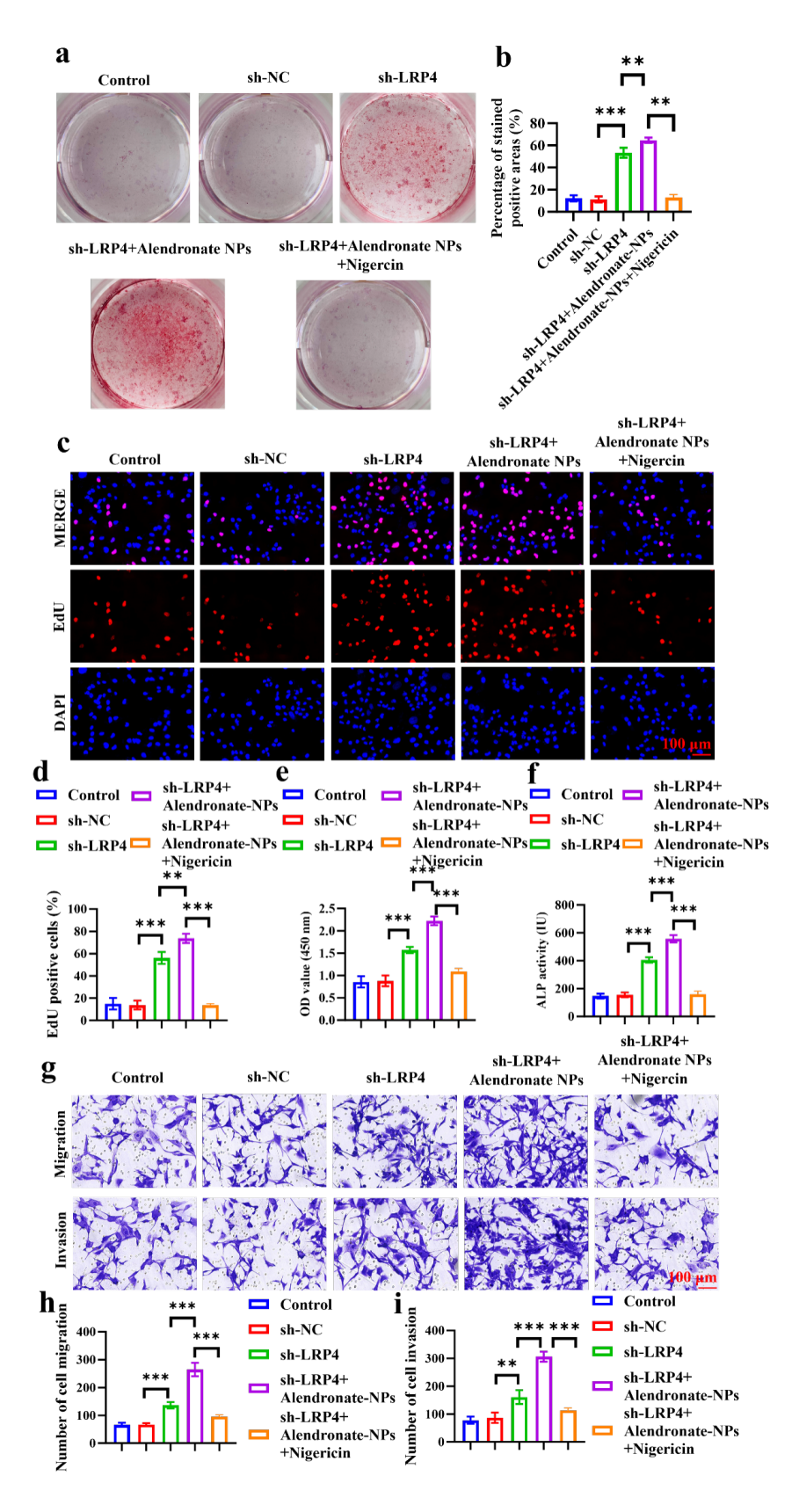


Fig. 8. Nigercin inhibits MC3T3-E1 cell viability and osteogenic differentiation. (a,b) Alizarin red S staining MC3T3-E1 cells. (c,d) EdU staining MC3T3-E1 cells. Scale bar =  $100 \ \mu m$ . (e) Proliferation rate of MC3T3-E1 cells assessed by CCK-8 assay. (f) ALP activity. (g-i) The migration and invasion of MC3T3-E1 cells were analyzed by Transwell assay. Scale bar =  $100 \ \mu m$ . N = 3. \*\*p < 0.01, \*\*\*p < 0.001. The images were plotted using GraphPad Prism 8.0 software.



group, the fracture space was larger, and the fracture callus and fracture space were significantly reduced in the alendronate and alendronate-NPs, especially in the alendronate-NPs. This finding indicated the potential of alendronate to promote fracture healing. Compared with the model + alendronate group, alendronate-NPs demonstrated better fracture-healing ability (Fig. 7a). Bone formation and metabolism are significantly influenced by ALP. Assessing the activity of ALP in serum reflects the degree of bone maturation and formation, thereby indicating the impact of alendronate on fracture healing. The ALP activity test showed that serum ALP activity in the model + alendronate group notably increased compared with the model group (p < 0.05). Serum ALP activity in the model + alendronate-NPs group was significantly higher than that in the model + alendronate group (p < 0.001; Fig. 7b). Additionally, immunohistochemical results for collagen protein (Fig. 7c,d) showed that the expression of collagen protein was lowest in the model group compared with that in the control group (p < 0.01). Compared with the model group, the expression of collagen protein significantly increased after treatment with alendronate and alendronate-NPs (p < 0.05). The treatment effect of alendronate-NPs was superior to that of alendronate alone.

The Wnt/β-Catenin Pathway Inhibitor Nigercin Inhibited MC3T3-E1 Cell Viability and Osteogenic Differentiation

We silenced LRP4 and Nigercin to further discuss the role of Wnt/beta-catenin and LRP4 in fracture healing. Fig. 8a,b shows that silencing LRP4 and combining alendronate NPs significantly promoted osteogenic differentiation of MC3T3-E1 cells, whereas Nigercin significantly inhibited the osteogenic differentiation of MC3T3-E1 cells (p < 0.001). In Fig. 8c-f, sh-LRP4 + alendronate-NPs promoted cell-proliferation viability and ALP activity (p < 0.01), but Nigercin reversed this trend (p < 0.001). Finally, Fig. 8g-i also confirmed that sh-LRP4 + Alendronate-NPs promoted cell invasion, whereas Nigercin inhibited MC3T3-E1 cell invasion (p < 0.001).

#### **Discussion**

Alendronate, a frequently prescribed medication for osteoporosis, slows down bone loss primarily by suppressing osteoclast activity [25,26]. Nevertheless, recent research indicates that alendronate may play a possible part in enhancing the mending of fractures [27]. Alendronate can enhance the healing of fractures by blocking LRP4 and stimulating the Wnt/ $\beta$ -catenin pathway. This feature offers a fresh outlook on the creation of innovative strategies for treating fractures. We examined if alendronate can stimulate the Wnt/ $\beta$ -catenin pathway and enhance fracture healing by inhibiting LRP4 via a rat fracture model. The experimental findings indicated that alendronate decreased the levels of LRP4 but increased the levels of Wnt4, pGSK3 $\beta$ , and  $\beta$ -catenin, which were downstream targets

of the Wnt/ $\beta$ -catenin pathway to enhance fracture healing. This phenomenon was aligned with the established role of LRP4 as a suppressor of the Wnt/ $\beta$ -catenin signaling pathway. Therefore, our results strongly linked alendronate to fracture healing.

The Wnt/ $\beta$ -catenin pathway is a significantly preserved pathway for signal transduction with a crucial function in diverse biological processes, encompassing cellular growth, specialization, and programmed cell death [2,28]. The Wnt/ $\beta$ -catenin signaling pathway is activated during fracture healing, stimulating the differentiation and maturation of osteoblasts, thereby improving their capacity to form bone. Furthermore, the Wnt/β-catenin pathway can decrease bone resorption by inhibiting osteoclast formation and activity [29]. Wnt/ $\beta$ -catenin signaling reportedly promotes fracture healing in rats. Pan et al. [30] found that apigenin activates Wnt/ $\beta$ -catenin signaling to promote the osteogenic differentiation of mesenchymal stem cells and accelerate fracture healing. Zheng et al. [31] found that osthole induces osteogenic and angiogenic coupling in bone-marrow mesenchymal stem cells through the Wnt/βcatenin pathway, thereby accelerating the healing of osteoporotic fractures. Combined with our research results, I also demonstrated the key role of the Wnt/ $\beta$ -catenin pathway in fracture healing, as further verified by the inhibitor Nigercin.

In this study, a new mechanism was suggested for the promotion of fracture healing by alendronate. This mechanism involved the blocking of LRP4 and the subsequent activation of the Wnt/ $\beta$ -catenin pathway. Our findings offered experimental support for the potential use of alendronate in enhancing fracture healing. However, the specific impact of alendronate on LRP4 expression remains unclear, necessitating further investigation into its targets and mechanisms of action. Although the rat fracture model used in this study provided valuable insights, the differences in the fracture healing between rats and humans warrant further validation in large animal models that closely resemble clinical conditions. To further investigate the potential impact of alendronate on fracture healing, future studies should prioritize the following aspects: analyze the inhibitory mechanism of alendronate on LRP4 and its correlation with the Wnt/ $\beta$ -catenin pathway; conduct additional clinical trials to confirm the effectiveness and safety of alendronate in promoting fracture healing; and explore the potential benefits of combining alendronate with other therapeutic methods to enhance the overall therapeutic outcomes of fracture healing.

However, several limitations in our current study should be acknowledged. First, our findings were based on a rat fracture model, which may not fully represent the complexities of human fracture healing processes. Second, we demonstrated the involvement of the Wnt/ $\beta$ -catenin pathway, but other potential signaling pathways influencing fracture healing warrant investigation. The optimal dosage,

duration, and timing of alendronate-NP treatment need further optimization for clinical applications. Future studies should focus on conducting large animal studies, investigating additional molecular mechanisms, and evaluating longterm safety profiles. Despite these limitations, our findings provided valuable insights into the therapeutic potential of alendronate-NPs in fracture healing and established a foundation for future clinical translation.

#### **Conclusions**

Alendronate-NPs indirectly activated the Wnt/ $\beta$ -catenin pathway by inhibiting LRP4, offering a new explanation for their role in promoting fracture healing. Further investigation is needed to explore the significance of LRP4 as an important controller of the Wnt/ $\beta$ -catenin pathway in bone development and disease.

#### **List of Abbreviations**

Wnt, Wingless-Int-Integrated;  $\beta$ -catenin, catenin; LRP4, lipoprotein receptor-related protein 4; PDI, polydispersity index; EE, encapsulation efficiency; DL, drug loading; SEM, scanning electron microscopy; FBS, fetal bovine serum; cDNA, complementary DNA; qRT, quantitative reverse-transcription; PCR, polymerase chain reaction; PCNA, proliferating cell nuclear antigen; Runx2, runt-related transcription factor 2; OCN, osteocalcin; Wnt4, Wingless-type MMTV integration site family, member 4; GSK- $3\beta$ , glycogen synthase kinase 3 beta; GAPDH, glyceraldehyde 3-phosphate dehydrogenase; CCK-8, cell counting kit-8; ALP, alkaline phosphatase; HE, hematoxylin-eosin; IOD, integrated optical density; NPs, nanoparticles; OPN, osteopontin; mRNA, messenger ribonucleic acid; TUNEL, terminal deoxynucleotidyl transferase-mediated dUTP nick end labeling; PLGA, poly(lactic-co-glycolic acid); PEG, polyethylene glycol; shRNA, short hairpin RNA; PBS, phosphate buffer saline; DMEM, Dulbecco's modified Eagle medium; DAPI, 4',6-diamidino-2-phenylindole; BCA, bicinchoninic acid assay; PVDF, polyvinylidene fluoride; HRP, horseradish peroxidase.

# **Availability of Data and Materials**

The datasets used and/or analysed during the current study were available from the corresponding author on reasonable request.

#### **Author Contributions**

ZWS and YHS designed the study. JPG, YHS and QLZ collected and analyzed the data. ZWS and XYL participated in drafting the manuscript. All authors conducted the study and contributed to critical revision of the manuscript for important intellectual content. All authors made substantial contributions to the conception or design of the work. All authors gave final approval of the ver-

sion to be published. All authors participated fully in the work, took public responsibility for appropriate portions of the content, and agreed to be accountable for all aspects of the work in ensuring that questions related to the accuracy or completeness of any part of the work were appropriately investigated and resolved.

## **Ethics Approval and Consent to Participate**

This study has been approved by the ethics committee of Yantaishan Hospital, Approval No. 2024018. All animal procedures were performed in accordance with the Guidelines for the Care and Use of Laboratory Animals of Yantaishan Hospital.

### Acknowledgments

Not applicable.

# **Funding**

Not applicable.

#### **Conflict of Interest**

The authors declare no conflict of interest.

#### References

- [1] Merlijn T, Swart K, Van der Horst H, Netelenbos J, Elders P. Fracture prevention by screening for high fracture risk: a systematic review and meta-analysis. Osteoporosis International: a Journal Established as Result of Cooperation between the European Foundation for Osteoporosis and the National Osteoporosis Foundation of the USA. 2020; 31: 251–257. https://doi.org/10.1007/s00198-019-05226-w.
- [2] Haffner-Luntzer M. Experimental agents to improve fracture healing: utilizing the WNT signaling pathway. Injury. 2021; 52: S44—S48. https://doi.org/10.1016/j.injury.2020.11.051.
- [3] Dong J, Xu X, Zhang Q, Yuan Z, Tan B. The PI3K/AKT pathway promotes fracture healing through its crosstalk with Wnt/β-catenin. Experimental Cell Research. 2020; 394: 112137. https://doi.org/10. 1016/j.yexcr.2020.112137.
- [4] Zhao C, Yu T, Dou Q, Guo Y, Yang X, Chen Y. Knockout of TLR4 promotes fracture healing by activating Wnt/β-catenin signaling pathway. Pathology, Research and Practice. 2020; 216: 152766. https://doi.org/10.1016/j.prp.2019.152766.
- [5] Cao R, Chen P, Wang H, Jing H, Zhang H, Xing G, et al. Intrafusal-fiber LRP4 for muscle spindle formation and maintenance in adult and aged animals. Nature Communications. 2023; 14: 744. https://doi.org/10.1038/s41467-023-36454-8.
- [6] Geng S, Paul F, Kowalczyk I, Raimundo S, Sporbert A, Mamo TM, et al. Balancing WNT signalling in early forebrain development: The role of LRP4 as a modulator of LRP6 function. Frontiers in Cell and Developmental Biology. 2023; 11: 1173688. https://doi.org/10.3389/fcell.2023.1173688.
- [7] Al-Qattan MM, Alkuraya FS. Cenani-Lenz syndrome and other related syndactyly disorders due to variants in LRP4, GREM1/FMN1, and APC: Insight into the pathogenesis and the relationship to polyposis through the WNT and BMP antagonistic pathways. American Journal of Medical Genetics. Part A. 2019; 179: 266–279. https://doi.org/10.1002/ajmg.a.60694.
- [8] Davidson G. LRPs in WNT Signalling. Handbook of Experimental Pharmacology. 2021; 269: 45–73. https://doi.org/10.1007/164\_2021\_526.
- [9] Tian J, Shao J, Liu C, Hou HY, Chou CW, Shboul M, et al. Defi-



- ciency of lrp4 in zebrafish and human LRP4 mutation induce aberrant activation of Jagged-Notch signaling in fin and limb development. Cellular and Molecular Life Sciences: CMLS. 2019; 76: 163–178. https://doi.org/10.1007/s00018-018-2928-3.
- [10] Bullock WA, Hoggatt AM, Horan DJ, Elmendorf AJ, Sato AY, Bellido T, et al. Lrp4 Mediates Bone Homeostasis and Mechanotransduction through Interaction with Sclerostin In Vivo. iScience. 2019; 20: 205–215. https://doi.org/10.1016/j.isci.2019.09.023.
- [11] Yu H, Zhang J, Liu X, Li Y. microRNA-136-5p from bone marrow mesenchymal stem cell-derived exosomes facilitates fracture healing by targeting LRP4 to activate the Wnt/β-catenin pathway. Bone & Joint Research. 2021; 10: 744–758. https://doi.org/10.1302/2046-3758.1012.BJR-2020-0275.R2.
- [12] Katchkovsky S, Chatterjee B, Abramovitch-Dahan CV, Papo N, Levaot N. Competitive blocking of LRP4-sclerostin binding interface strongly promotes bone anabolic functions. Cellular and Molecular Life Sciences: CMLS. 2022; 79: 113. https://doi.org/10.1007/ s00018-022-04127-2.
- [13] Cummings SR, Santora AC, Black DM, Russell RGG. History of alendronate. Bone. 2020; 137: 115411. https://doi.org/10.1016/j.bo ne.2020.115411.
- [14] Kendler D, Chines A, Clark P, Ebeling PR, McClung M, Rhee Y, et al. Bone Mineral Density After Transitioning From Denosumab to Alendronate. The Journal of Clinical Endocrinology and Metabolis. 2020; 105: e255–e264. https://doi.org/10.1210/clinem/dgz095.
- [15] Iacobellis G. Treating the Bone to Protect the Heart: Potential Newer Mechanisms and Targets. The American Journal of the Medical Sciences. 2019; 357: 451–452. https://doi.org/10.1016/j.amjms.2019. 02.001.
- [16] Patel D, Saxena B. Decoding osteoporosis: Understanding the disease, exploring current and new therapies and emerging targets. Journal of Orthopaedic Reports. 2025; 4: 100472. https://doi.org/10.1016/j.jorep.2024.100472.
- [17] Dayanandan AP, Cho WJ, Kang H, Bello AB, Kim BJ, Arai Y, et al. Emerging nano-scale delivery systems for the treatment of osteoporosis. Biomaterials Research. 2023; 27: 68. https://doi.org/10.1186/s40824-023-00413-7.
- [18] Cheng X, Wei J, Ge Q, Xing D, Zhou X, Qian Y, et al. The optimized drug delivery systems of treating cancer bone metastatic osteolysis with nanomaterials. Drug Delivery. 2021; 28: 37–53. https://doi.or g/10.1080/10717544.2020.1856225.
- [19] Sharma AR, Lee YH, Bat-Ulzii A, Chatterjee S, Bhattacharya M, Chakraborty C, et al. Bioactivity, Molecular Mechanism, and Targeted Delivery of Flavonoids for Bone Loss. Nutrients. 2023; 15: 919. https://doi.org/10.3390/nu15040919.
- [20] Fahmy SA, Mahdy NK, Al Mulla H, ElMeshad AN, Issa MY, Azzazy HME. PLGA/PEG Nanoparticles Loaded with Cyclodextrin-Peganum harmala Alkaloid Complex and Ascorbic Acid with Promising Antimicrobial Activities. Pharmaceutics. 2022; 14: 142. https://doi.org/10.3390/pharmaceutics14010142.
- [21] Krüger TB, Syversen U, Herlofson BB, Lian AM, Reseland JE. Targeting a therapeutically relevant concentration of alendronate for *in vitro* studies on osteoblasts. Acta Odontologica Scandinavica. 2022; 80: 619–625. https://doi.org/10.1080/00016357.2022.2072522.
- [22] Qian D, Zhang Q, He CX, Guo J, Huang XT, Zhao J, et al. Hai-Honghua medicinal liquor is a reliable remedy for fracture by pro-

- motion of osteogenic differentiation via activation of PI3K/Akt pathway. Journal of Ethnopharmacology. 2024; 330: 118234. https://doi.org/https://doi.org/10.1016/j.jep.2024.118234.
- [23] Wang K, Zhou C, Li L, Dai C, Wang Z, Zhang W, et al. Aucubin promotes bone-fracture healing via the dual effects of antioxidative damage and enhancing osteoblastogenesis of hBM-MSCs. Stem Cell Research & Therapy. 2022; 13: 424. https://doi.org/10. 1186/s13287-022-03125-2.
- [24] Iles B, Ribeiro de Sá Guimarães Nolêto I, Dourado FF, de Oliveira Silva Ribeiro F, de Araújo AR, de Oliveira TM, et al. Alendronate sodium-polymeric nanoparticles display low toxicity in gastric mucosal of rats and Ofcol II cells. NanoImpact. 2021; 24: 100355. https://doi.org/https://doi.org/10.1016/j.impact.2021.100355.
- [25] Manzano-Moreno FJ, Ramos-Torrecillas J, de Luna-Bertos E, Illescas-Montes R, Arnett TR, Ruiz C, et al. Influence of pH on osteoclasts treated with zoledronate and alendronate. Clinical Oral Investigations. 2019; 23: 813–820. https://doi.org/10.1007/ s00784-018-2505-z.
- [26] de Faria LP, Sueyoshi G, de Oliveira TC, Holliday LS, Arana-Chavez VE. Effects of Alendronate and Dexamethasone on Osteoclast Gene Expression and Bone Resorption in Mouse Marrow Cultures. The Journal of Histochemistry and Cytochemistry: Official Journal of the Histochemistry Society. 2022; 70: 169–179. https://doi.org/10.1369/00221554211063519.
- [27] Pedersen AB, Heide-Jørgensen U, Sørensen HT, Prieto-Alhambra D, Ehrenstein V. Comparison of Risk of Osteoporotic Fracture in Denosumab vs Alendronate Treatment Within 3 Years of Initiation. JAMA Network Open. 2019; 2: e192416. https://doi.org/10.1001/jamanetworkopen.2019.2416.
- [28] Wang J, Yang C, Kong F, Zhang Z, Ji S, Sun G. Cebpb Regulates Skeletal Stem Cell Osteogenic Differentiation and Fracture Healing via the WNT/β-Catenin Pathway. Stem Cells International. 2022; 2022: 2091615. https://doi.org/10.1155/2022/2091615.
- [29] Mudri D, Bilić Ćurčić I, Meštrović L, Mihaljević I, Kizivat T. Hyperthyroidism and Wnt Signaling Pathway: Influence on Bone Remodeling. Metabolites. 2023; 13: 241. https://doi.org/10.3390/metabol3020241.
- [30] Pan FF, Shao J, Shi CJ, Li ZP, Fu WM, Zhang JF. Apigenin promotes osteogenic differentiation of mesenchymal stem cells and accelerates bone fracture healing via activating Wnt/β-catenin signaling. American Journal of Physiology. Endocrinology and Metabolism. 2021; 320: E760–E771. https://doi.org/10.1152/ajpendo.00543.2019.
- [31] Zheng S, Hu G, Zheng J, Li Y, Li J. Osthole accelerates osteoporotic fracture healing by inducing the osteogenesis-angiogenesis coupling of BMSCs via the Wnt/β-catenin pathway. Phytotherapy Research: PTR. 2024; 38: 4022–4035. https://doi.org/https://doi.org/10.1002/ ptr.8267.

**Editor's note**: The Scientific Editor responsible for this paper was Juerg Gasser.

**Received**: 30th December 2024; **Accepted**: 28th April 2025; **Published**: 26th June 2025

